Journal of the European Ceramic Society xxx (xxxx) xxx

Contents lists available at ScienceDirect

Journal of the European Ceramic Society

journal homepage: www.elsevier.com/locate/jeurceramsoc

Cold sintering of the ceramic potassium sodium niobate, $(K_{0.5}Na_{0.5})NbO_3$, and influences on piezoelectric properties

Kosuke Tsuji [a,b], Zhongming Fan [a], Sun Hwi Bang [a,b], Sinan Dursun [a], Susan Trolier-McKinstry [a,b], Clive A. Randall [a,b,*]

[a] Materials Research Institute, Department of Materials Science and Engineering, The Pennsylvania State University, University Park, PA, 16802, USA
[b] Department of Materials Science and Engineering, The Pennsylvania State University, University Park, PA, 16802, USA

ARTICLE INFO

Keywords:
Cold sintering process
Potassium-sodium niobate
Piezoelectric ceramics
Lead-Free piezoelectrics
Low temperature sintering

ABSTRACT

Cold Sintering was applied to densify a Potassium-Sodium Niobate solid solution composition, $0.5KNbO_3$-$0.5NaNbO_3$ (KNN); the process uses a transient chemical sintering aid, moderate pressure (400 MPa), and temperatures between 230–300 °C to obtain ceramics of ~92 to 96 % theoretical density. Typically, sintering temperatures between ~1000–1050 °C are required to density KNN using conventional methods. In this paper, the densification was investigated during heating, particularly the shrinkage in the first 60 min of the cold sintering process. The low-field dielectric and electrical properties of the resulting ceramics were found to be comparable to conventionally sintered KNN. Electric fields up to 80 kV/cm could be applied, however the ceramics showed pinched hysteresis loops, even after poling over a wide range of temperatures and electric fields. A Rayleigh analysis was used to investigate domain dynamics and high reversible permittivity. The irreversible behavior was an order of magnitude lower than in conventionally sintered KNN, likely associated with defect pinning of ferroelectric domains. A Transmission Electron Microscopy (TEM) study revealed a high density of line defects in most grains; dislocations in the grains limit poling and domain wall movement, thus suppressing both the piezoelectric properties and the hysteresis. Furthermore, TEM observations indicated crystalline grain boundaries that were faceted with terrace kink ledges. These observations point to the importance of the initial powder optimization and grain boundary diffusion when using cold sintering to prepare ceramics that are intended to show bulk cooperative properties such as ferroelectricity. The impact of limited high temperature homogenization of bulk diffusional processes is discussed.

1. Introduction

Piezoelectric ceramics are widely utilized in sensors, actuators, transducers, transformers and various other devices. The observation of high piezoelectric coefficients at the morphotropic phase boundary in lead zirconate titanate ceramics has made these ceramics commercially important. However, more recently, interest in lead-free piezoelectric ceramic materials has grown due to concerns over the impact of lead on the environment and the human body. The KNN-based material system is a promising source of lead-free piezoelectrics because of its high piezoelectric and coupling constants [1,2].

Ferroelectricity was first reported in the alkali niobate system by Bell Laboratories as early as 1949 [3]. In 1954, Pepinsky et al. detailed the structural and electrical properties of KNN through extended studies of the $KNbO_3$-$NaNbO_3$ solid solution system [4]; Egerton et al. [5] then reported on the piezoelectric properties. However, processing conditions have limited the densification of KNN with good functional properties [5,6], likely due to alkaline carbonates, precursors of KNN, that are volatile and sensitive to humidity [7]. Additionally, the sintering window is close to KNN's liquidus gap, which causes compositional shifts during sintering [8–10]. Therefore, numerous strategies to improve the microstructure, density, and properties of KNN materials have been reported, including hot pressing [11], liquid phase sintering aids [12,13], spark plasma sintering [14,15] microwave sintering[16] and atmospheric conditions (using lower partial pressures of oxygen, for example) [17].

It has been reported that various ceramic oxides can be sintered below 300 °C by the cold sintering process (CSP) [18,19]. This is

* Corresponding author at: Materials Research Institute, Department of Materials Science and Engineering, The Pennsylvania State University, University Park, PA, 16802, USA.
E-mail address: car4@psu.edu (C.A. Randall).

https://doi.org/10.1016/j.jeurceramsoc.2021.10.002
Received 20 July 2021; Received in revised form 23 September 2021; Accepted 5 October 2021
Available online 7 October 2021
0955-2219/

realized by the pressure-solution creep between ceramic particles promoted by the addition of an appropriate solvent and uniaxial pressure; sintering is completed efficiently at a low temperature in a short time. Alkaline molten salts appear to be a very effective solvent for the cold-sintering of many oxides [20]. In the case of $BaTiO_3$, which has the same perovskite structure as KNN, very dense microstructure and a high dielectric constant were obtained at 300 °C with the addition of alkaline molten salts [21]. Based on these results, the sintering of KNN using a similar approach appears to be promising. In this study, a similar approach to that used in the $BaTiO_3$ system was applied to KNN ceramics. KNN (K/Na = 1.0) was chosen to understand the densification of KNN ceramics by CSP. These NaOH-KOH fluxes are designed around the eutectic composition and overcome the incongruent dissolution problems of the perovskite structure and enables the dissolution and reprecipitation process of cold sintering to proceed. The properties of cold-sintered ceramics were then characterized and compared with those of KNN ceramics sintered by conventional methods. The discussion is extended to understanding the processing-structure-property relationships, with an emphasis on processing-derived lattice defects.

2. Experimental Procedure

K_2CO_3 (99.997 %, Alfa Aesar), Na_2CO_3 (99.95–100.05 %, Alfa Aesar), Nb_2O_5 (99.9 %, Alfa Aesar) were dried at 200 °C for > 2 weeks prior to use. Then, the powders were mixed with a stoichiometric composition of $(K_{0.5},Na_{0.5})NbO_3$ and ball-milled with 3 mm of YSZ in ethanol for 24 h. After being dried at 120 °C for 12 h, the powders were calcined twice at 800 °C for 4 h followed by 24 h of ball milling after each calcination. The average particle size was ≈ 180 nm after this processing. The calcined powder was mixed with 4–10 vol % mixture of NaOH (Fisher Scientific, >98 %) and KOH (Fisher Scientific, 99.99 %) in 50:50 M ratio of Na to K. The volume fraction was estimated based on the respective density of the powders: KNN (4.5 g/cm^3), NaOH (2.13 g/cm^3). After being thoroughly grounded, the powder mixture was uniaxially pressed at 400 MPa and heated to 150−300 °C for 0–3 hours. Sintering time is defined as the total time at the maximum temperatures (isothermal dwell time, t_{dwell}). The Nickel foils were used to cover specimens to minimize contamination from the die. The linear displacement was monitored using a contact sensor (Keyence GT-H32) under semi-automatic hydraulic pressure [22]. The change in linear displacement was compared between KNN powder and KNN powder with 10 vol% of NaOH-KOH flux. The specimens were dried at 200 °C, and then densities of pellets were measured geometrically. A density of 4.51 g/cm^3 was used to calculate relative density of the sintered KNN ceramics [23]. Phase purity was investigated by X-ray diffraction (XRD, Empyrean, PANalytical) with a scan rate of 0.067°/s using Cu Kα radiation. The microstructures were observed by Field Emission Scanning Emission Microscopy (ZEISS GeminiSEM, Carl Zeiss). Prior to the microstructure observation, all specimens were polished with 50 nm diamond paste. Then, the surface was etched with a diluted HCl-HF solution for 5–10 seconds. More than 350 grains were counted; grain sizes were estimated by the linear intercept method [24]. The initial particle size was also estimated from SEM micrograph using the equivalent circle diameter [25]. 80 nm thick Pt was sputter-deposited (Q150R Plus, Quorum) and used for the electrical measurements. Dielectric properties were measured with a HP 4284A precision LCR meter. The polarization-field (*P-E*) hysteresis loop was measured using a Sawyer-Tower circuit with a Trek Model 30/20 high voltage amplifier system (Trek, Inc., Lockport, NY). The KNN pellets were poled under different conditions (electric field, E_p,: 40−70 kV/cm, poling temperature, T_p: R.T. to 100 C, poling time, t_p,:10 and 30 min). After poling, the field was maintained during cooling to room temperature in order to minimize backswitching and maximize the poled state. The direct piezoelectric coefficient d_{33} was determined by a Berlincourt meter (PM 300, Piezotest Pte. Ltd.). The subgrain defects were visualized by Transmission Electron Microscopy (TEM) in a Talos F200X (FEI), with the specimen prepared using Focused Ion Beam (Scios 2, FEI).

3. Results and discussion

Fig. 1**(a)** shows the relative densities of cold-sintered KNN ceramics with different sintering temperatures and amounts of hydroxide flux based on the pellet geometry. It was found that higher sintering temperature and a higher amount of NaOH-KOH flux resulted in higher relative densities within the experimental window in this study. Good dielectric properties (ε_r ~500, tanδ~ 2.5 % at 1 kHz) and insulation resistance (>10^{11} Ω cm were obtained with the sintering temperature as low as 230 °C with 10 vol% of NaOH-KOH flux, and significant improvement was not observed for other conditions. These properties are comparable to the high-quality specimen values reported in references [10,26]. Therefore, further characterization focuses on specimens sintered at 230 °C under 400 MPa of uniaxial pressure for 3 h of isothermal dwell with 10 vol% of NaOH-KOH flux.

Fig. 1**(b)** demonstrates the change in linear displacement and temperature profile as a function of time. Three different cases were tested, using the same sintering temperature of 230 °C and applied pressure of 400 MPa, to accurately interpret the displacement evolution. The calibration indicates no powder and transient phase was placed in the sintering die. Hence, the resulting displacement of 0.30 mm was reasonably due to the axial thermal expansion of sintering instrument. When only KNN powder was placed for the same experiment, the resulting displacement change was reduced down to 0.23 mm. Although the axial thermal expansion is still a dominant factor that affects the degree of displacement, the radial thermal expansion and powder packing possibly cause the shrinkage. However, for the case of KNN powder with 10 vol.% of NaOH + KOH flux, the resulting displacement change of 0.03 mm and the presence of an inflection point clearly suggest that other factors may largely influence the displacement such as densification and possibly some extrusion. According to the relative density measurement, the proposed flux can drive the densification of KNN powder, indicating that the pore volume is sufficiently removed under the cold sintering condition. Therefore, the removed pore volume pertains to the linear shrinkage. Regarding the extrusion, some mass can be extruded from the sintering die through the small but a finite gap between sintering die punch and sleeve. However, when input and output weights were compared, the difference was less than 5%, which is considered to be a minor factor. Note that the relative density at 0-minute isothermal dwell was 93.8 %, so the displacement does not noticeably change during the isothermal dwell. The highly repeatable temperature profiles confirm that the possible presence of thermal artifact is minimum in the given analysis.

Fig. 2 compares cold sintering to the other sintering methods. There have been many attempts to lower the sintering temperatures of KNN, but most of them have required a temperature of 1000 °C or higher (Fig. 2). Therefore, it is noteworthy that the present work achieves the same or higher degree of densification at 230 °C. As is widely reported, for high temperature sintering, the sintering temperature, T_s, relative to the melting temperature, T_m, generally lies in the range $0.85 < T_s/T_m < 0.95$ [6,11–13,16,17]. In contrast, for cold sintering, it is typical for $T_s/T_m < 0.2$, and is shown here for KNN.

Fig. 3 shows SEM micrographs of the initial powder and cold-sintered KNN ceramics with different isothermal holds at a temperature of 230 °C with dwell time (t_{dwell} = 0 and 180 min). The sintered ceramics shows dense microstructures. The cuboidal grains in Fig. 3**(b, c)** represent typical grain morphologies observed in conventionally sintered KNN ceramics [2,27]. As can be seen, the porosity is minor, even with a very short sintering time (t_{dwell} = 0 min). No significant microstructure change is seen following the isothermal hold at the cold sintering temperature. Average grain sizes were calculated to be 304 and 297 nm for samples sintered for 0 and 3 h holds, respectively (Fig. 3**(d, e)**). As the initial grain size was about 240 ± 14 nm (Fig. 3**(a)**), some degree of grain growth occurred simultaneously with densification

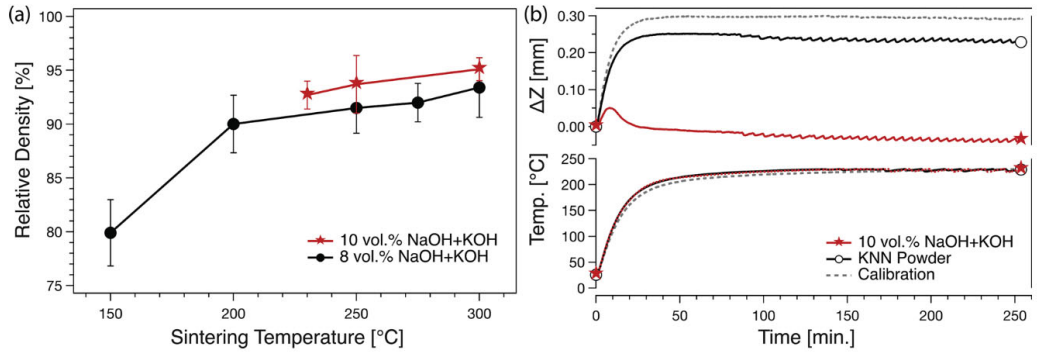

Fig. 1. Effect of sintering temperature and amount of NaOH-KOH flux on the relative densities of KNN ceramics. A uniaxial pressure (400 MPa) and sintering time (3 h) were used for all conditions. The pressure is fixed before in raising of the temperature, and so is deemed constant over the sintering runs (b) Change in linear displacement (ΔZ) and temperature profile (Temp.) in a function of time. Positive ΔZ indicates expansion and negative ΔZ means shrinkage.

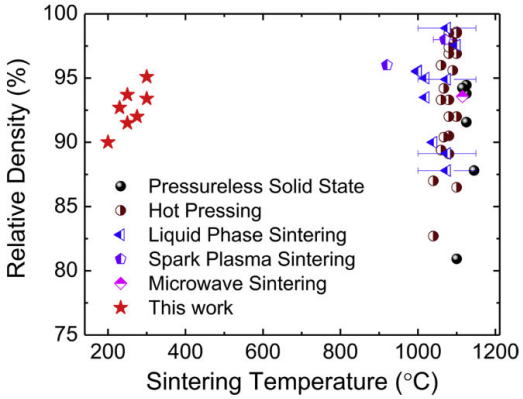

Fig. 2. Comparison of property-processing relationship by different sintering method (Pressureless Solid State Sintering (SSS), [6,11] Hot Pressing (HP) [11], Liquid Phase Sintering (LPS) [12,13,17], Spark Plasma Sintering (SPS) [14,15], Microwave Sintering(MWS) [16], Cold Sintering Process (CSP, this work).

during the non-isothermal segments of the cold sintering process (i.e. first 75 min. in Fig. 1**(b)**). This is driven by the pressure-assisted solution-reprecipitation diffusional mechanisms enabled with the the NaOH-KOH sintering aid. Previous work of CSP in $BaTiO_3$ with the aid of REAXFF molecular dynamics models and other experiments including transmission electron microscope studies showed that the slightly hydrated hydroxide flux controls metastable cation complexes in the fluxes and drives the dissolution and reprecipitation process [28].

Fig. 4 shows XRD patterns for the initial powder and as-CSP KNN pellet sintered at 230 °C for 3 h. The diffraction patterns of both initial powder and cold-sintered pellet are identified as orthorhombic crystal structure at room temperature, as expected [29,30]. No secondary phase was detected by X-ray diffraction. It is then considered that the perovskite phase is preserved during dissolution-precipitation in the CSP.

As the insulation resistivity was high enough for poling ($>10^{11}$ Ω cm, the direct piezoelectric coefficient (d_{33}) was measured with different poling conditions. Fig. 5**(a)** shows the d_{33} as a function of poling field (E_p) with fixed poling time (t_p) and temperature (T_p). The initial condition (T_p = 50 °C, E_p = 40 kV/cm t_p = 10 min) was chosen based on previous studies. However, the resulting d_{33} was small (~10 pC/N), indicating that the ceramics cannot realize a fully stabilized poled state. As the E_p increased, the d_{33} value also gradually increased, but it was still limited to less than 30 pC/N. The poling condition was further investigated by increasing the temperature, as shown in Fig. 5 **(b)**. While d_{33} increased slightly with poling temperatures above 50 °C, it was limited to < 30 pC/N. A significant difference in the maximum d_{33} was not seen with E_p of 40 or 60 kV/cm when T_p was sufficiently high. The obtained value of d_{33} is much lower than the typical value of KNN ceramics in the reported literature (d_{33} = 110–160 pC/N) [10]. The poling conditions used in this study should be sufficient to pole undoped KNN [10,31–33]. Additionally, considering that the dielectric properties are comparable to reported values, it is unlikely that d_{33} was limited by the impurity phase (e.g. undetected secondary phase or hydroxide flux).

As the piezoelectric coefficient is directly related to the polarization (d_{33} =$2Q_{33}P_s\varepsilon$), the polarization-electric field (*P-E*) characteristics were investigated. Fig. 6 shows a *P-E* hysteresis loop of cold-sintered KNN. The maximum electric field of 80 kV/cm used in Fig. 6 is much higher than the coercive field of KNN ceramics. However, the loop is pinched and did not show polarization saturation. The value of the remanent polarization (P_r) in the unpoled CSP KNN ceramics was < 2 μC/cm^2, a much lower value than typically found in KNN (P_r = 20–30 μC/cm^2), and a coercive field (E_c = 15–20 kV/cm) [10]. A pinched hysteresis loop is often seen when the ferroelectric domain wall state is characterized by random internal electric fields (possibly due to defect dipoles) [34,35]. Note that neither increasing the electrical field up to 100 kV/cm, nor cycling the a.c. field up to 10^3 times, nor a combination of those, led to an opening of the *P-E* loop.

Rayleigh analysis provides insight into extrinsic contribution and an indirect assessment of associated defect pinning sites. The Rayleigh law describes the field dependence of the dielectric permittivity as follows [36];

$$\varepsilon' = \varepsilon_{init} + \alpha_e E_0 \quad (1)$$

$$P(E) = (\varepsilon_{init}\alpha_e + E_0)E \pm \frac{\alpha_e}{2}(E_0^2 - E^2) \quad (2)$$

where ε_{init} is the dielectric permittivity resulting from intrinsic lattice response and reversible motion of domain walls. α_e is the irreversible Rayleigh parameter, E is the applied a.c. electric field, and E_0 is its amplitude (E=E_0 sin(ωt)). The second term of Eq. (1) represents the irreversible contribution tot he total dielectric permittivity.

Fig. 7(a) shows the field dependence of the dielectric permittivity below the coercive field (E_c). The measured dielectric permittivity shows a clear linear relationship with the amplitude of the a.c. electric field, as expected from Eq. (1). The Rayleigh parameters, α_e and ε_{init}, are obtained from the slope and intercept of the linear fitting in Fig. 7**(a)** (α_e = 8.4 × 10^{-5} (m/V) and ε_{init} = 513). The low-field *P-E* hysteresis was calculated with Eq. (2) using the obtained Rayleigh coefficients. Fig. 7 **(b)** shows a good agreement the calculated hysteresis with the measured value, indicating that the low-field polarization characteristics of KNN ceramics can be well described by the Rayleigh law. The Rayleigh coefficient of 8.4 × 10^{-5} (m/V) in cold-sintered KNN is significantly lower

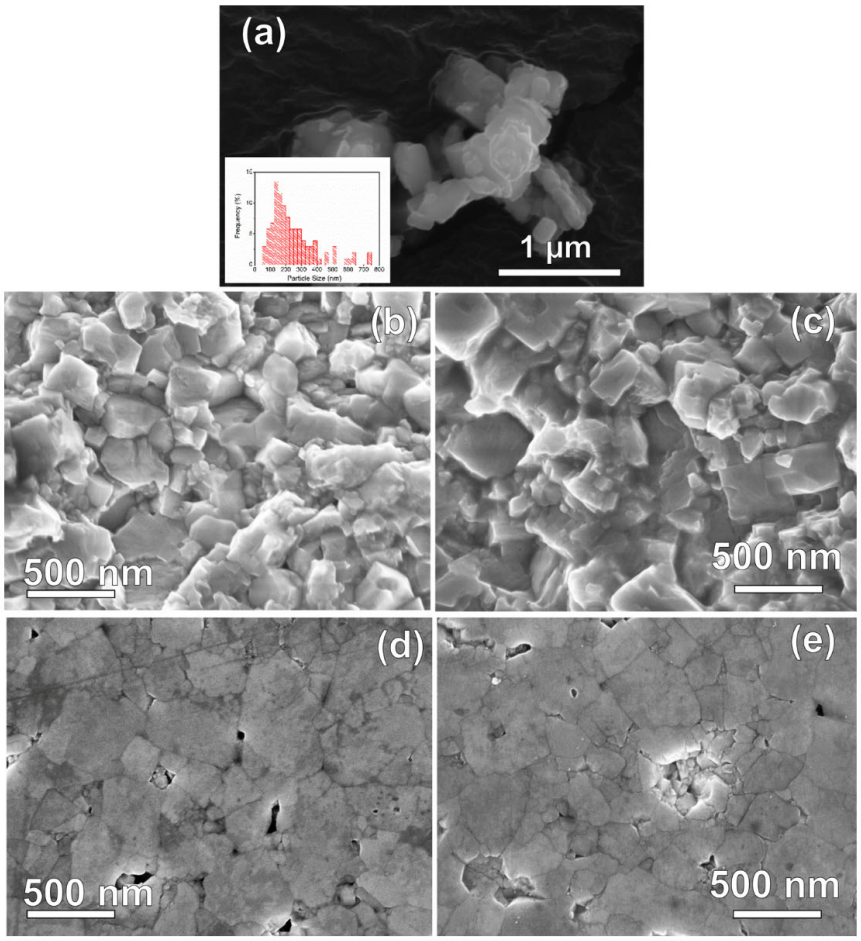

Fig. 3. SEM micrograph of (a) KNN initial powder, and size distribution as an insert, and (b-e) cold sintered ceramics. (b,c) fracture surface (d,e) polished surface of the cold-sintered ceramics. The sintering time at 230 °C is $t_{dwell} = 0$ min (b,d), $t_{dwell} = 180$ min (c,e).

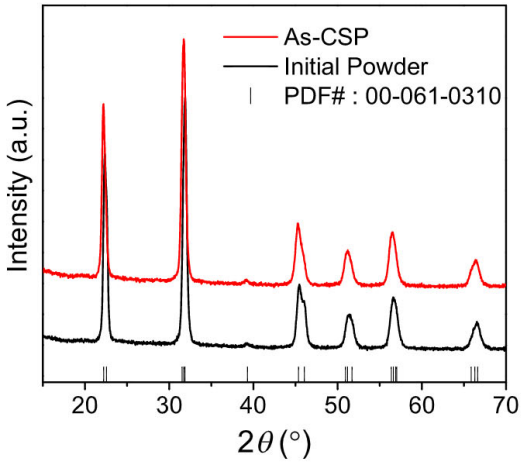

Fig. 4. XRD patterns of the initial KNN powder and as-CSP KNN pellet. Black bars on the bottom represent peak position of $K_{0.5}Na_{0.5}NbO_3$ (PDF#: 00-061-0310). [29].

than the reported value in high-temperature sintered KNN ceramics (*c.f.* $\alpha_e = 1.08 \times 10^{-3}$ (m/V)) [37]. The lower α_e indicates the irreversible domain wall motion is less active. The extrinsic contribution calculated from the ratio of measured permittivity to the second term of Eq. (1) at 5 kV/cm was 7.5 % and 61 % for cold-sintered and conventionally sintered KNN ceramics, respectively [37,38].

The irreversible domain wall motion requires overcoming an energy barrier that originates from pinning (often due to defects) in the specimen (Fig. 8**(a)**). The lower Rayleigh coefficient indicates that the potential wells are deeper, but broader in cold-sintered KNN ceramics than in conventionally sintered KNN ceramics (Fig. 7**(b,c)**). As a result, the extrinsic contribution was significantly suppressed, and a low d_{33} was observed. The origin of the strong pinning site is not clear. It is possible that the increased interface (grain boundary) inhibited domain wall motion, as is known with grain size effects with PZT [39]. In the present study, the grain size is much smaller than commonly reported in KNN ceramics, and thus, the interfacial effect should be high. Indeed, a similar observation, showing high ε_r with low P_r and/or low $d_{33,}$ has already been reported in fine-grain $BaTiO_3$ ceramics [40]. A strong pinning effect of grain boundaries has been also reported in PZT thin films [41,42]. An additional possibility that is also important to consider is the possibility of a high point defect concentration. Some point defects can be introduced due to imperfect crystallization during CSP in grain boundary regions or in the bulk of grains due to powder synthesis, with

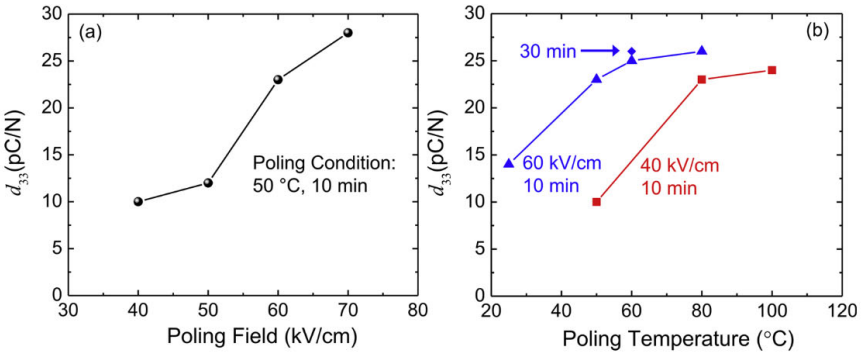

Fig. 5. Piezoelectric coefficient of the cold-sintered KNN ceramics with different poling conditions. Specimens used for poling studies were prepared at 230 °C with 10 vol% of NaOH-KOH under 400 MPa of uniaxial pressure.

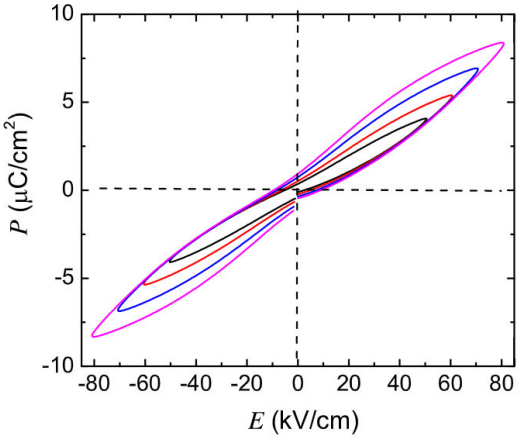

Fig. 6. *P-E* hysteresis of the cold-sintered KNN ceramics prepared at 230 °C with 10 vol% of NaOH-KOH under 400 MPa of uniaxial pressure.

insuffecient homogeneity and crystallization in the calcination step, or dislocation generation in the milling of powders.

To understand the nature of the defects, a bright field diffraction contrast imaging of the grain structures of the CSP KNN ceramics was made. Fig. 9**(a)** shows highly defective grains with many dislocations; it is speculated that may have disrupted the irreversible motion of ferroelectric domain walls. The central grain is darker, as it is undergoing a strong diffraction condition, and this reveals both the high density of defects and also the grain boundary outline. The grain boundary is also seen to be made up of many terrace kinks, or steps reflecting the epitaxial growth, that were previously noted in the cold sintering of Na_2MoO_7 [18]. Fig. 9**(b)** shows a high-resolution image with lattice fringes in adjacent crystallites. The interface is atomically sharp with no glassy phases between the grain boundaries. We can also observe the interlocking of the steps across the grain boundary. It is apparent that there are no grain boundary glass phases that would reduce the permittivity and degrade poling. Therefore, KNN ceramics cold sintered under the conditions utilized here have a high concentration of line defects, crystalline grain boundaries, and small grain sizes. It is inferred that although high-density ceramics with crystalline grain boundaries can be prepared by CSP, the properties are limited by grain growth and the preponderance of grain boundary rather than bulk diffusion. As a result, defects that are inherent in the starting powders are retained throughout CSP. Thus, it will be critical in the future to carefully design the calcination and milling steps so that powders with low initial defect densities are utilized for cold sintered piezoelectrics.

The importance of mixing and solid-state reactions and the evolution of high crystallinity in conventionally sintered KNN ceramics has been reported [43]. Thong et al. reported improvements in the powder crystallinity with a calcination temperature ~1000 °C [44]. They used a structuring of KNN powders with a dielectrophoretic assembly method in a polymer undergoing in situ cross-linking. To obtain high performance, Deutz et al. used a rigorous calcination condition (1050 °C for 3 h and 950 °C for 20 h) for KNN powder to achieve excellent piezoelectric properties in the KNN-PDMS composites [45]. The relatively lower calcination temperature was used in this study for better densification

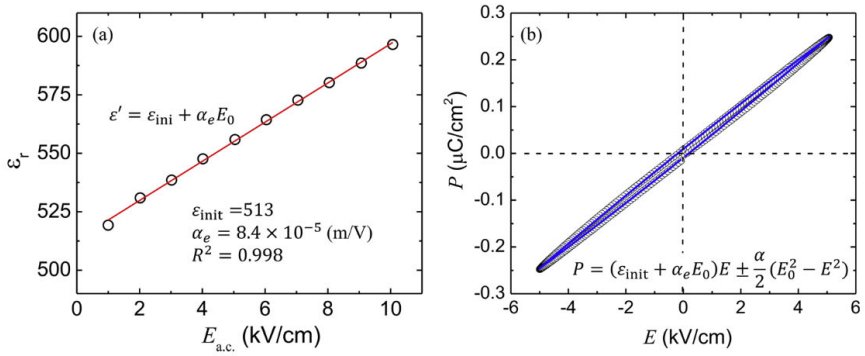

Fig. 7. (a) Field dependence of dielectric permittivity at 100 Hz, (b) *P-E* hysteresis at 5 kV/cm at 100 Hz of the cold-sintered KNN ceramics prepared at 230 °C with 10 vol.% of NaOH-KOH under 400 MPa of uniaxial pressure. Circle: Measured values, Blue line: calculated value (For interpretation of the references to colour in this figure legend, the reader is referred to the web version of this article).

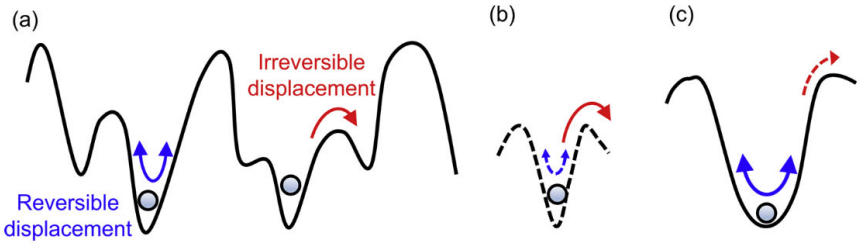

Fig. 8. (a) Potential energy landscape for the domain wall motion in ferroelectric ceramics.[42] Proposed local potential well for the conventionally sintered KNN (b) and the cold-sintered KNN (c).

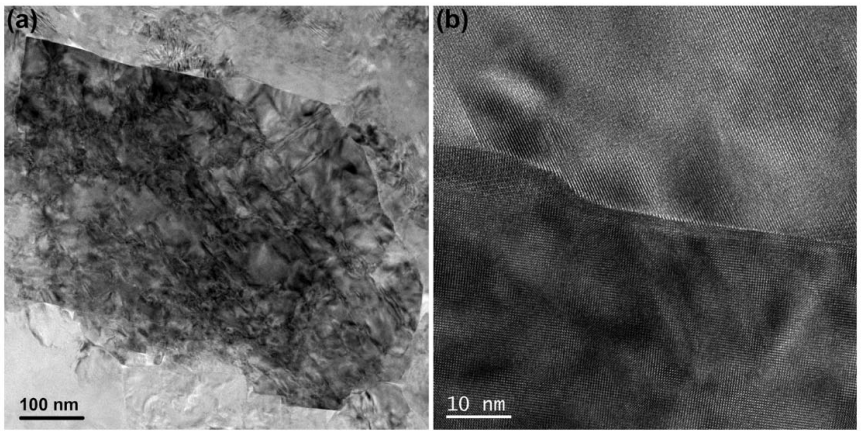

Fig. 9. (a) A representative grain with high density of linear defects; (b) a representative kinked grain boundary with good crystallinity in the cold-sintered KNN ceramics prepared at 230 °C with 10 vol% of NaOH-KOH under 400 MPa of uniaxial pressure.

with fine particles, but future studies need to focus on the quality of the initial powder [44].

4. Conclusions

The densification of KNN piezoelectric ceramic materials can be readily accomplished via cold sintering at temperatures $T_s/T_m < 0.2$ (T_s: Sintering temperature, T_m: Melting temperature of KNN). The final densities are over 92 % with the use of NaOH-KOH at approximately 200 °C, at 400 MPa. The densification is largely complete after the first hour. The grain size is ~200 nm and is limited in coarsening at isothermal holds at these temperatures. According to X-ray diffraction, the phase purity is maintained through the cold sintering steps. The low field dielectric permittivity is similar to conventionally sintered KNN ceramics. High electric field strengths can be applied ~ 80 kV/cm, without high losses, suggesting that there is reasonable dielectric strength and control over nonlinear conduction mechanisms. Despite these observations, high poling fields do not provide high piezoelectric performance. A Rayleigh analysis showed difficulty moving the domain walls; this is reflected in lower nonlinear coefficients. TEM observation revealed a high concentration of line defects in the grains. These are believed to originate from the imperfect crystallization at the calcination step. The bulk defect states did not change under cold sintering, as the major diffusion processes that drive densification are surface and grain boundary diffusion pathways. The bulk diffusion processes that participate in conventional sintering are limited under cold sintering, so the residual defect states and concentrations in the calcined powders are not changed. Future work for piezoelectric ceramics will need to consider not only the grain boundary interfaces, but also the defect types and concentrations in the powders to be utilized in cold sintering. Clearly, in the case of cold sintering and piezoelectric properties, the dislocation concentration will be a very important consideration, given its role in domain and/or domain wall pinning.

Declaration of Competing Interest

There are no conflicts to declare.

Acknowledgements

This material is based upon work supported in part by the National Science Foundation, as part of the Center for Dielectrics and Piezoelectrics under Grant Nos. IIP-1841453 and 1841466. We also thank the members of the many companies that continue to offer support and ideas to drive this work. The author (K.T.) also thanks Dr. A. Ndayishimiye for helpful discussions, Dr. L. Gao for experimental guidance, and Kim Trolier and Joanne Aller for proof-reading.

References

[1] Y. Saito, H. Takao, T. Tani, T. Nonoyama, K. Takatori, T. Homma, T. Nagaya, M. Nakamura, Nature 432 (2004) 84.
[2] T.R. Shrout, S.J. Zhang, J. Electroceramics 19 (2007) 111.
[3] B.T. Matthias, Phys. Rev. 75 (1949) 1771.
[4] G. Shirane, R. Newnham, R. Pepinsky, Phys. Rev. 96 (1954) 581.
[5] L. Egerton, D.M. Dillon, J. Am. Ceram. Soc. 42 (1959) 438.
[6] M. Kosec, D. Kolar, Mater. Res. Bull. 10 (1975) 335.
[7] B. Malič, J. Koruza, J. Hreščak, J. Bernard, K. Wang, J.G. Fisher, A. Benčan, Materials (Basel). 8 (2015) 8117.
[8] S. Zhang, R. Xia, H. Hao, H. Liu, T.R. Shrout, Appl. Phys. Lett. 92 (2008) 2006.
[9] U. Flückiger, H. Arend, J. Cryst. Growth 43 (1978) 406.
[10] S. Zhang, H.J. Lee, C. Ma, X. Tan, J. Am. Ceram. Soc. 94 (2011) 3659.
[11] R.E. Jaeger, L. Egerton, J. Am. Ceram. Soc. 45 (1962) 209.

[12] M. Matsubara, T. Yamaguchi, W. Sakamoto, K. Kikuta, T. Yogo, S.I. Hirano, J. Am. Ceram. Soc. 88 (2005) 1190.
[13] J. Bernard, A. Benčan, T. Rojac, J. Holc, B. Malič, M. Kosec, J. Am. Ceram. Soc. 91 (2008) 2409.
[14] R. Wang, R. Xie, T. Sekiya, Y. Shimojo, Mater. Res. Bull. 39 (2004) 1709.
[15] M. Bah, F. Giovannelli, F. Schoenstein, G. Feuillard, E. Le Clezio, I. Monot-Laffez, Ceram. Int. 40 (2014) 7473.
[16] M. Feizpour, H. Barzegar Bafrooei, R. Hayati, T. Ebadzadeh, Ceram. Int. 40 (2014) 871.
[17] K. Kobayashi, Y. Doshida, Y. Mizuno, C.A. Randall, J. Am. Ceram. Soc. 95 (2012) 2928.
[18] J. Guo, H. Guo, A. Baker, C.A. Randall, Angew. Chem. Int. Ed. Engl. 128 (2015) 1.
[19] J. Guo, R. Floyd, S. Lowum, J. Maria, T. Herisson de Beauvoir, J. Seo, C.A. Randall, Annu. Rev. Mater. Res. 49 (2019) 275.
[20] S. Lowum, R. Floyd, J.P. Maria, J. Mater. Sci. 55 (2020) 12747.
[21] K. Tsuji, A. Ndayishimiye, S. Lowum, R. Floyd, K. Wang, M. Wetherington, J. P. Maria, C.A. Randall, J. Eur. Ceram. Soc. 40 (2020) 1280.
[22] R. Floyd, S. Lowum, J.P. Maria, Rev. Sci. Instrum. 90 (2019), 055104.
[23] L. Egerton, C.A. Bieling, Am. Ceram. Soc. Bull. 47 (1968) 1151.
[24] ASTM E112-13, ASTM Int. 1 (2013).
[25] ASTM International 15 (2003) 2.
[26] Y. Saito, H. Takao, Ferroelectrics 338 (2006) 17.
[27] P. Kabakov, P. Kabakov, C. Dean, V. Kurusingal, Z. Cheng, H.Y. Lee, S. Zhang, J. Mater. Chem. C 8 (2020) 7606.
[28] A. Ndayishimiye, M.Y. Sengul, D. Akbarian, Z. Fan, K. Tsuji, S.H. Bang, A.C.T. Van Duin, C.A. Randall, Nano Lett. 21 (2021) 3451.
[29] J. Tellier, B. Malic, B. Dkhil, D. Jenko, J. Cilensek, M. Kosec, Solid State Sci. 11 (2009) 320.
[30] D.W. Baker, P.A. Thomas, N. Zhang, A.M. Glazer, Appl. Phys. Lett. 95 (2009) 1.
[31] G.H. Haertling, J. Am. Ceram. Soc. 50 (1967) 329.
[32] E. Hollenstein, D. Damjanovic, N. Setter, J. Eur. Ceram. Soc. 27 (2007) 4093.
[33] Y. Saito, H. Takao, in Ferroelectrics, 2006, pp. 17–32.
[34] M.E. Lines, A.M. Glass, Principles and Applications of Ferroelectrics and Related Materials, Oxford University Press, 2001.
[35] G. Robert, D. Damjanovic, N. Setter, Appl. Phys. Lett. 77 (2000) 4413.
[36] D.V. Taylor, D. Damjanovic, Appl. Phys. Lett. 73 (1998) 2045.
[37] K. Kobayashi, Y. Doshida, Y. Mizuno, C.A. Randall, J. Am. Ceram. Soc. 95 (2012) 2928–2933.
[38] D.V. Taylor, D. Damjanovic, J. Appl. Phys. 82 (1997) 1973.
[39] C.A. Randall, N. Kim, J.-P. Kucera, W. Cao, T.R. Shrout, J. Am. Ceram. Soc. 81 (1998) 677.
[40] L. Egerton, S.E. Koonce, J. Am. Ceram. Soc. 38 (1955) 412.
[41] D.M. Marincel, H. Zhang, A. Kumar, S. Jesse, S.V. Kalinin, W.M. Rainforth, I. M. Reaney, C.A. Randall, S. Trolier-McKinstry, Adv. Funct. Mater. 24 (2014) 1409.
[42] P. Bintachitt, S. Jesse, D. Damjanovic, Y. Han, I.M. Reaney, S. Trolier-McKinstry, S. V. Kalinin, Proc. Natl. Acad. Sci. U. S. A. 107 (2010) 7219.
[43] B. Malic, D. Jenko, J. Holc, M. Hrovat, M. Kosec, J. Am. Ceram. Soc. 91 (2008) 1916.
[44] H.C. Thong, A. Payne, J.W. Li, Y.Y.S. Cheng, J.L. Jones, K. Wang, Acta Mater. 211 (2021), 116833.
[45] D.B. Deutz, N.T. Mascarenhas, J.B.J. Schelen, D.M. de Leeuw, S. van der Zwaag, P. Groen, Adv. Funct. Mater. 27 (2017) 1.